Science Ascend

From October 8-14, 2024!

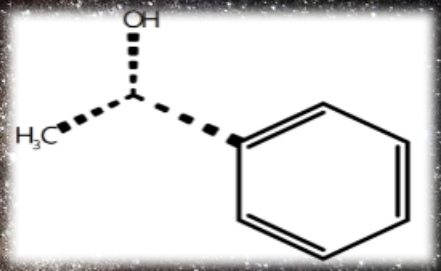

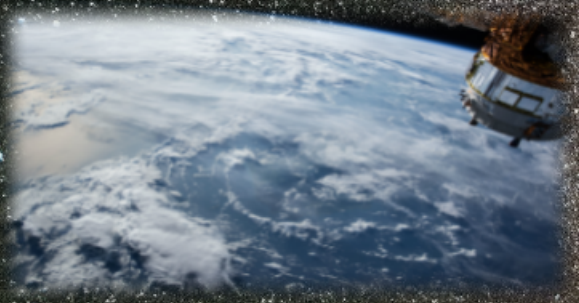

cout<<solutions;

ISSN: 3062-0090
FIRE Araştırma Eğitim Ltd. Şti., Vol:1, Issue:6

Science Ascend

Rising to New Heights of Discovery!

Science Ascend teleports you to the frontiers of science. It compiles and discuss the scientific research preprints from arXiv, bioRxiv, chemRxiv just from the previous week to be cognizant of the *state-of-the-art* of knowledge in astrophysics, chemistry, environmental chemistry, remote sensing, and applied statistics/data science. Light from the *Science Ascend* will keep brightening the dark horizon beyond the limits of our comprehension. FIRE Araştırma Eğitim Ltd. Şti. guarantees the weekly publication and dissemination of this journal, and make it available for everyone at most fifteen days after its publication freely.

Publisher: FIRE Araştırma Eğitim Ltd. Şti.
Media: Online Journal
Responsible person: Yasin Güray Hatipoğlu
Editor-in-chief: Yasin Güray Hatipoğlu
Editor: Yasin Güray Hatipoğlu
Frequency: Once a week
Address: Yıldızevler Mah. Kişinev Cad. No:10 Çankaya/Ankara/Türkiye
Website: https://fire-ae.github.io

This issue: October 14, 2024

Volume: 1

Issue Number: 6

Bilim Yükselişi

Keşfin Yeni Yükseklerine Ulaşmak!

Science Ascend sizi bilimin sınırlarına ışınlar. Astrofizik, kimya, çevre kimyası, uzaktan algılama ve uygulamalı istatistik/veri bilimi alanlarındaki bilgi birikiminin *en son durumu* hakkında bilgi sahibi olmak için arXiv, bioRxiv, chemRxiv'den sadece bir önceki haftaya ait bilimsel araştırma ön baskılarını derler ve tartışır. *Bilim Yükselişi*'nden gelen ışık, kavrayışımızın sınırlarının ötesindeki karanlık ufku aydınlatmaya devam edecektir. FIRE Araştırma Eğitim Ltd. Şti. bu derginin haftalık olarak yayınlanmasını, dağıtılmasını ve yayınlandıktan en geç on beş gün sonra ücretsiz olarak herkesin erişimine açılmasını garanti eder.

Yayıncı: FIRE Araştırma Eğitim Ltd. Şti.
Ortam: Online Journal
Sorumlu Kişi: Yasin Güray Hatipoğlu
Yazı İşleri Müdürü: Yasin Güray Hatipoğlu
Editör: Yasin Güray Hatipoğlu
Yayınlanma Sıklığı: Haftada bir kez
Adres: Yıldızevler Mah. Kişinev Cad. No:10 Çankaya/Ankara/Türkiye
Website: https://fire-ae.github.io

Bu sayı: 14 Ekim 2024

Cilt: 1

Sayı Numarası: 6

Contents

Foreword

Greetings everyone!

In the sixth issue of *Science Ascend*, the usual 5 articles were again compiled and written by Güray Hatipoğlu, and for the sixth article *Selected Works from Machine Learning*, the guest author Oğuz Demirtaş prepared the arXiv preprint reviews. The reason why this issue got out quite later than what it should have been is mostly my personal challenges in the preceding weeks. Unfortunately, FIRE Araştırma Eğitim Ltd. Şti. is affected by this quite a lot, since there is no human resource buffer to prevent this. Nevertheless, preprint screening and reference recording steps were streamlined to reduce the time lost for these parts of this work and instead focus on actual reading-reviewing. See you all at the next issue!

Güray Hatipoğlu

Last week in Astrophysics

Author: Yasin Güray Hatipoğlu

The preprints summarized here were published between October 8 - October 14, 2024. These are from arXiv's astro.EP cross-fields without high-energy main cross-list papers.

Astrochemistry

Hänni et al.[1] investigated the high-resolution mass spectra (HR-MS) measurements from the 67P/Churyumov-Gerasimenko comet with a specific focus on dimethylsulfide (DMS).

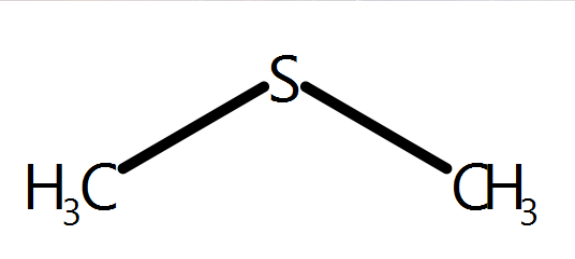

Figure 1: Dimethylsulfide molecule

DMS is one of the critical molecules related to the *life presence*. There has not been a natural abiotic source for this molecule and it may imply a biogenesis had it discovered in any other exoplanets, such as its detection and subsequent controversies around K2-18b. Nevertheless, the researchers of this study reported that rather than the isomer ethanethiol, they actually detected DMS in this comet, indicating an abiotic source for the robust biosignature.

Stellar Systems - Populations - Clusters

Sharma et al.[2] aimed to better understand the exoplanet evolution through the chemical abundances (C, N, O and alpha-elements[1] of Mg and Si and several abundance ratios of planet-hosting star atmosphere from the high-resolution spectra of 149 F, G, and K type dwarf and giant stars (and 1071 comparison sample stars without any detected planets). They utilized the Vilnius University Echelle Spectrograph on the 1.65 m Molėtai Observatory. They used the observations with the resolution modes 36000 and 68000, and the spectroscopy ranged from 400 to 880 nm wavelength. Their signal-to-noise ratios were between 75 and 200. For the determination of the stellar atmospheric parameters (effective temperature, surface gravity, microturbulence velocity, and metallicity) they combined DAOSPEC and MOOG codes. The abundances were calculated with the TURBOSPECTRUM code and they utilized MARCS stellar atmosphere models in this procedure. They used galpy Python package for the kinematics and orbital properties and the UniDAM (unified tool to estimate distances, ages, and masses) to determine stellar ages. In order to check the extent of the difference (or if there is any significant difference) between the planet hosts and the control sample, they applied the Kolmogorov-Smirnov and Anderson-Darling tests. They reported interesting correlations between the stellar parameters, being a planet host or not, age, and other relevant characters.

Diamond and Parker[3] studied the formation of the Jupiter mass binary objects in the Orion Nebula Cluster (ONC) theoretically. The way they approach it includes a photoerosion mechanism (by the Lyman continuum radiation from massive stars) of normally binary or higher-order multiple systems generating fragmented protostellar cores. Luhman et al.[4], on the other hand, utilized the JWST/NIRSpec observations of 22 Brown Dwarfs in the ONC. A considerable discussion and measurements were made on proplyds (ionized protoplanetary disks), and their sample included proplyds (Source 69, 117 near and below the hydrogen burning limit and a protostellar brown dwarf (Source 126).

Single Star System (Star, Exoplanet)

Cooke and Madhusudhan[5] made an intriguing study on K2-18 b considering the photochemical modeling and whether or not it is an uninhabited or inhabited Hycean world [2]. For the pressure-temperature profiling and initial states, they used PICASO and Photochem, as well as VULCAN and FastChem (the last pair was for the mini-Neptunes, while for a Hycean, only VULCAN was used). They reported that the previously favored mini-Neptune was not compatible with the retrievals, but the inhabited HYcean scenario was a better match.

Liu et al.[6] tried to constrain the shape of Kepler-51d with the James Webb Space Telescope (JWST) Near Infrared Spectroscopy (NIRSpec) data. The observation was done with the following settings: The bright object time-series mode

[1] These are produced within the stellar core via alpha particle captures starting from the carbon element, along several others more.

[2] Hycean is hydrogen + ocean, a hydrogen-rich atmosphere and a water ocean beneath. The inhabited and uninhabited difference is a marked methane (CH_4) difference, where the former has a higher, biogenic methane source

(BOTS) of NIRSpec, CLEAR filter, PRISM disperser, SUB512 subarray, and the NRSRAPID readout pattern for 15 hours of science data duration. They reduced the data with the standard jwst 1.15.1 following no. 29 JWebbinars, and the generated white light curve from the full wavelength range was reduced with the Eureka! package in addition to the jwst package to compare the oblateness (ellipticity) constraints. In the oblateness modelling, JoJo computed the oblate planet lightcurve with the quadratic limb darkening profile, and the **celerite2** generated the light curve baseline (Matern-3/2) and red noises with a Gaussian process. They reported that the shape of Kepler-51d is probably spherical, excluding the oblateness values higher than 0.08 within 30 degrees of planet-spin alignment, and 0.2 if the misalignment is higher.

Noack et al.[7] prepared the 'Surface and Interiors chapter for the first edition of the Encyclopedia of Astrophysics, including the composition and interior structure of exoplanets and the feedback between the exoplanet's interior and surface, synthesizing the accumulated knowledge and linking them between the star, its exoplanets, their atmospheres, surfaces, and the interior structures. Thus, the focus was on rocky planets, especially the super-Earths and mini-Neptunes.

Conzo et al.[8] confirmed the discovery of the TIC 393818343 c with the differential photometry method using ground-based telescopes (Toni Scarmato's Observatory MPC-L92 - Briatico, Italy; Nastro Verde Observatory MPC-C82 - Sorrento, Italy; and LCO-Telescopes Observatory MPC-Z21 - Teide, Spain.) and synthetic radial curve analysis with Forecaster package.

Casewell et al.[9] studied the GD1400, white dwarf-brown dwarf binary system, with the UVES Echelle Spectrometer in the UT2 of the ESO VLT for radial velocity measurements, the STE4 CCD imager and UCT high-speed camera at the South African Astronomical Observatory for the optical wavelength time-series photometry, the Son OF Isaac on the New Technology Telescope La Silla with the $J, H, and K_s$ filters for the near-infrared, and for the mid-infrared region ALLWISE catalog was utilized. They reported a lower-than-previous day-night temperature differential for the brown dwarf and discussed how this system of the ZZ Ceti pulsator white dwarf and a brown dwarf came it to be.

Damiano et al.[10] summarized the methods developed to suppress exozodiacal disk and relevant noises in the hypothetical starshade-produced exoplanet system images from the Starshade Exoplanetary Data Challenge[3]. The team Quartus Engineered removed the background with the Independent Component Analysis[4] technique and worked on the resulting image with point-spread functions (PSFs). The other team, Mississippi State University used the PSF subtraction, disk modelling, and multi-epoch differential imaging methods to separate non-exoplanetary signals. Other teams and reports can be downloaded from the challenge website. They cautioned the added errors with the approaches chosen and false positives/negatives.

Elms et al.[11] presented 17 new and cooler white dwarfs as spectrophotometric flux standards for the Hubble Space Telescope. For the study, they employed HST, Gaia DR3, 2MASS, and WISE data. They provided the model for these 17 WD here.

Lalande et al.[12] utilized machine learning techniques and found that k-nearest neighbors Kernel Density Estimates (kNNxKDE) to estimate exoplanet mass and make imputation. They used the NASA Exoplanet Archive data with mostly missing planetary mass values, but still a non-negligible part containing all planet mass, planet radius, orbital period, planet equilibrium temperature, stellar mass, and number of known planets in the corresponding system. Other than kNNxKDE, they also used MissForest, Generative Adversarial Imputation Nets, Multiple Imputation Chained Equations, and kNN-Imputer. In the end, they generally found similar good performances for the random forest based MissForest and kNNxKDE, but preferred the latter as it provides a probability density instead of point estimates.

On the public interaction of exoplanet science, Deeg[13] reported interesting results on citizen science, STEM education interests, and the impact of the information that there are "other Earths" beyond our Solar System. Similarly, Wright et al.[14] reviewed the developments in the SETI in 2022, categorizing them under searches, instrumentation and methodology, target and frequency selection, development of technosignatures, theory of extraterrestrial intelligences, and social aspects.

Placco et al.[15] made high-resolution (R approx. 100000) and signal-to-noise ratio (approx. 800) observations of BD+44°493. Primary observations were made with the WIYN 3.5-meter Telescope NEID echelle spectrograph, but they also compiled many radial velocity data, atmospheric parameters, Gaia DR3, K magnitude of the 2MASS, and complementary chemical abundances from Subaru/HDS, HST/STIS, and HST/COS. They confirmed that it was born out

[3]The webpage for the challenge is here.

[4]The application of a whitening technique like PCA, then iteratively ensuring that the resulting components are statistically independent of each other.

of the remnants of a 20.5 solar mass metal-free star in the early universe, among many other interesting and more constrained values.

Terry et al.[16] analyzed the Keck-I telescope adaptive optics images of the microlensing event MOA-2011-BLG-262 from the Galactic Bulge. In the data reduction step, they used Keck Adaptive Optics Imaging Data Reduction Pipeline, and DAOPHOT-II for the PSF Fitting Photometry. They found that among the previously postulated two scenarios, the one with the very low mass star and a planetary companion in the galactic bulge was closer to explain the observation results. More specifically, they reported a host star mass of 0.19 ± 0.03 solar mass and planetary companion mass of 28.92 ± 4.75 Earth mass in 7.49 ± 0.91 kiloparsecs of distance. They also stated that with the transverse velocity of 541.31 ± 65.75 km s^{-1}, it was the highest velocity exoplanet system as of that time (October 11, 2024).

Exoplanet Atmospheres

Kirk et al.[17] studied the hot Jupiter WASP-15b[5] with the JWST NIRSpec via G395H[6] grating and F290LP[7] filter combination. They observed a single transit of WASP-15b on January 26, 2024, for 7.72 hours (685 integrations). They reduced the data in three different ways: with Tiberius, and Eureka! using two different parameter values. Then, they interpreted the spectra obtained from these pipelines with the petitRADTRANS 1D forward model and compared them to the BeAR (Bern Atmospheric Retrieval) and PLATON retrievals. In addition to these 1D models, 3D Met Office Unified Model was also used for making a 3D climate model and investigating spatial inhomogeneities. For the photochemical modelling, the updated C-H-N-O-S network from the VULCAN setup was used, especially for the subsequent discussion on sulfur chemistries. They reported the potential first detection of the OCS (carbonyl sulfide) molecule in an exoplanet atmosphere.

Valentine et al.[18] studied the atmosphere of the WASP-17b exoplanet in JWST-Telescope Scientist Team (TST) guaranteed time observations for the Deep Reconnaissance of Exoplanet Atmospheres through Multi-instrument Spectroscopy (DREAMS), with the Mid-Infrared Instrument Low Resolution Spectroscopy (MIRI/LRS) in the slitless mode on March 14, 2023. The observation had an exposure length of 9.92 hours (1276 integrations) in the FASTR1 fast readout pattern. They reduced the data with the ExoTiC-MIRI and Eureka!. For the atmospheric forward modelling they used the PICASO thermal equilibrium model version 3.2. This forward model result, then, was subtracted from the spectrum and the residuals were trying to be modelled with the dynesty and the Virga packages. For eclipse mapping, ThERESA was used. This approach permitted them to study WASP-17b's day-night temperature contrast and eclipse maps. Gressier et al.[19] further worked on WASP-17b, this time with the NIRISS (Near-Infrared Imager and Slitless Spectrograph) SOSS (Single Object Slitless Spectroscopy) Eclipse Spectroscopy. Their observation was on March 22, 2023, for 9.89 hours (720 integrations), with the SUBSTRIP256 subarray and GR700XD/CLEAR filter, and also 0.137-seconds and 10 integrations with the F277W filter. They reduced the data with the transitspectroscopy, supreme-SPOON, and Ahsoka[8] pipelines (Ahsoka was developed by them). The ATMO was used for the atmospheric forward modelling and TauREx v 3.1 and POSEIDON were used for the atmospheric retrieval analyses. The variations in the spectral reduction steps from the three aforementioned methods were reported to be mostly from how they handled the denoising, light curve creation, and overall differences of the Ahsoka and SupremeSPOON from the transitspectroscopy. There were interesting results regarding the water abundances, temperature profiles, and ways to handle the negative eclipse depth without introducing a Lucy-Sweeney-type bias[9].

Panwar et al.[20] used the archival Very Large Telescope (VLT) CRIRES (cryogenic high-resolution InfraRed Echelle Spectrograph) observations of the τ Boötis b to examine the water presence in its atmosphere with different stellar and telluric effect removal techniques and free-chemistry Bayesian atmospheric retrievals. They conducted a principal component analysis (PCA) on time series spectral data cubes to remove telluric and stellar effects as they assumed the wavelength-stationary state of these effects, while this is not so for the exoplanet. After that, they masked the insufficiently-detrended channels and optimized the choice of the number of principal components to retrieve. They chose this number (or more properly, the tuning parameter of the PCA method) according to the extent it suppresses the telluric lines (the higher the

[5]Naming comes from the detection via the 'Wide Angle Search for Planets, one in Spain (SuperWASP-North, one in South Africa (SuperWASP-South).

[6]G for grating, H for high-resolution, and 395 is related to the 3.95-micrometer wavelength

[7]F is for the filter, LP is low pass, 290 is related to the 2.90-micrometer wavelength

[8]The GitHub repository can be found in this link

[9]The procedures that force positive-definite parameters can result in this systematic bias towards more positive results than the actual cases

better). Then, they used cross-correlation functions to retrieve planetary component using the GENESIS, which is a numerical radiative transfer method that generates a spectrum according to the provided atmospheric temperature and chemical species information. After measuring the impact of the PCA on the exoplanet signal, they used Bayesian methods for the atmospheric retrieval step. In the end, they reported the carbon monoxide confirmation, marginal evidence for the water presence, and the details on the super-solar carbon/oxygen (C/O) ratio and sub-solar metallicity of the τ Boötis b.

Lavvas et al.[21] worked on the atmosphere of the GJ1214b using transit and eclipse[10] observations with the JWST/MIRI bands from 5 to 12 μm. They did not provide the code or data of this study, and reported the high likelihood of photochemical haze production, KCl, NaCl, ZnS-composed clouds, 2000-3000x solar metallicities, and also detected carbonyl sulfide (OCS).

Ashtari et al.[22] automated the light curve and spectroscopic data processing of transiting exoplanets with artificial intelligence (AI) based techniques, focusing on Hubble Space Telescope Wide Field Camera (WFC3). They chose parametric optimization, as opposed to the genetic one for the Eureka! optimization, which optimizes the range of values for the parameters one at a time and moves on to the next after that. They first confirmed the relationship between the equilibrium temperatures of hot Jupiters and the water-related band (1.4 μm). Moreover, a novel similar trend with cooler-shifted temperatures was found for the Neptune/sub-Neptunes, and there is a clear sky corridor between the planet mass vs. equilibrium temperature diagram, hinting at a relation between the metallicity and aerosol formation.

Kawahara et al.[23] expanded the previous JAX-based ExoJAX code, which can utilize Hamiltonian Monte Carlo method for the gradient-based Bayesian inference with the addition of atomic database access, a novel GPU memory-efficient opacity calculator (PreMODIT), and a systematic treatment of the radiative transfer[11]. Available molecular, metal, and continuum opacities are the ExoMol, HITEMP, HITRAN with or without air broadening, Kurucz and VALD3 metal lines, CIA, H-, Rayleigh scattering, and Cloud Mie scattering continuums. In addition to the pure absorption, their new code also incorporated the reflection and scattering cases and transmission spectrum. In the end, they demonstrated this for three cases: a clear sky T-dwarf emission Gl229B, a medium-resolution transmission spectroscopy of a hot Saturn WASP-39b, and the high-resolution reflection spectroscopy of Jupiter.

[10]Transit is when the exoplanet passes in front of the star it orbits, and eclipse is when the exoplanet passes behind its star, hence eclipsed by it.

[11]The GitHub repository for their new code can be found here.

Protoplanetary - Circumstellar Disks

Okmoto and Ida[24] simulated the solar system conditions and aimed to illuminate the excessive carbon depletion in the Earth and other rocky bodies of the Solar System. They started with a 100 au radius protoplanetary disk and conventional gas accretion model by turbulent diffusion without disk-wind driven accretion. The Monte Carlo simulations considered the amorphous hydrocarbons as refractory carbons, modeled the photolysis/oxidation, set the fragmentation limit velocity as 10 m/s for ice (1 m/s for silicates), considered the ice evaporation/recondensation, and carbon destruction rate (photolysis-oxidation). Unlike other studies, they were able to simulate the carbon-depleted conditions in the rocky components of the solar system with a lower fragmentation limit velocity of silicate than for the icy pebbles, and a considerably higher gas temperature in the upper, optically-thin layer near the mid-plane.

Schäfer et al.[25] conducted a simulation study to mitigate the lack of works in the literature on along-orbital direction filaments in the protoplanetary discs. They used the Pencil Code for the gas, dust, and planetesimal component simulations. Their main difference was comparatively much larger simulation sizes for the streaming instability[12], up to 6.4 gas scale heights in the plane. They reported a much better high-mass end of the initial mass function.

Tang et al.[26] studied sub-Neptune formation and proposed a new numerical model compared to the Ginzburg et al.[27]'s analytical modelling approach. The thermal contraction step started with the main equation that links the envelope luminosity to the rate of change of the specific entropy, and then, to the intrinsic luminosity, advective luminosity, radiogenic heating, and core temperature change. This was solved by a fifth-order ordinary differential equation (ODE) solver. The radiative atmosphere and adiabatic interior of the exoplanet were considered, and the planetary mass evolution was solved as another ODE problem. The Parker Wind, boil-off transition, and stellar extreme ultraviolet (XUV)-driven mass escape were also considered (XUV-related escape was not in the model). An important con-

[12]The hypothesis of planetesimal formation because of the drag within the gas disk spontaneously

clusion of this study was that highly-irradiated planets with smaller masses than 4 times Earth's mass should have another mechanism to drive gaseous envelope complete loss.

Nazari et al.[28] made a simulation study on the absence of exoplanet indicators in Class0/I protoplanetary discs. Firstly, they used models from the literature to simulate the evolution of the Class 0 protoplanetary disk to the Class II phase. Then, the RADMC-3D version 2.0 was used for the temperature calculations via radiative transfer computation at nine different times throughout the disk evolution. Works were also conducted on the minimum gap-opening mass for a forming planet in the Class 0/I cases, in addition to what was available as hydrodynamic simulation-based ones for Class II. They report cases where a specific mass planet opens an observable gap in Class II disks while not being able to open in earlier classes: a rocky planet at 1 au or a giant planet with 505 times Earth mass at 10 au.

Tyagi et al.[29] studied the protostellar accretion by observing the protostar HOPS 370 (OMC2-FIR3) with JWST NIRSpec/Integral Field Unit (IFU) and MIRI/Medium Resolution Spectroscopy (MRS). They reported the evidence for inner disk ice thermal processing and mapped the volatile ice species within approximately 80 au spatial resolution. They reported a highly inhomogeneous protostellar envelope.

Moon

Janhunen[30] reported that the lunar gravity anomalies might be beneficial on lunar sample capture by an active spacecraft without requiring a stream of materials from the Earth. The model used in the study was derived from the GRAIL mission, and it was the order-1200 spherical harmonic model of the lunar gravity field. There were three equatorial sites to hurl the projectile without a chemical propellant between 66 to 78 easting degrees.

Near-Earth Objects

Taylor et al.[31] studied the non-gravitational accelerations[13] on the identification challenges of near-eath objects (NEOs). Most importantly, an insufficient account of the non-gravitational accelerations on NEOs might lead to identify the same object as more than one distinct objects, i.e., false linking. They tested this on dark comet cases ($1998KY_{26}$ and $2003RM$)[14], synthetic data, and currently-known NEOs. For dark comets, they used the N-body integrator **ASSIST** code. Then, the results were generalized into the 100000 synthetic objects with the semimajor axis from [0.5, 4.2) au, eccentricity from [0, 1), orbital inclination [0, 15) degrees, argument of perihelion from [0, 360) degrees, longitude of ascending node from [0, 360) degrees[15], and true anomaly at epoch f_0 from [0, 360) degrees[16] distributions. After adding these, non-gravitational accelerations were added to see how much they change their on-sky positions from $[10^{-12}, 10^{-7}]$ au/d^2 distribution. They calculated the on-sky positions after integrating the equations for 1 and 10 years. After this simulation, the known NEO population from the Jet Propulsion Laboratory Small-Body Database was considered in the last section. The final part was checking the pair-linking of currently-in-use algorithm for NEOs and found that even though the objects with large non-gravitational accelerations ($\gtrsim 10^{-8}$) might be missed, otherwise the current algorithm was robust against non-gravitational accelerations.

Burnett et al.[32] rubble pile binary secondaries similar to the Didymos-Dimosphos[17]. They modeled the bigger, central of the duo as a single point mass and gravitational attraction while considering the secondary in much finer details as a rubble pile, with the Chrono-based N-body simulation architecture GRAINS. They elaborated on two cases: non-principal axis rotation and supersynchronous rotation. They reported tidal dissipation results non-negligibly different than the literature for similar cases, as well as other related tidal quantities.

Earth - Space relationship

Li et al.[33] reported the continuation of their multi-station meteor monitoring system in this paper. Their system upgrade increased the number of cameras to 4 from 1, reduced the field of view to 77° x 51°, the focal length became 8.0 mm, the RAM doubled to 16 GB, storage to 480

[13] Phenomena like outgassing in an unbalanced direction, radiolytic processes, etc. Observed activites (e.g., comae) may or may not be present.

[14] Asteroid naming convention. The first set of 4 numbers correspond to the discovery year, the first letter following is for the half month, January's first half starting from A. The remaining part is ordered alphabetically, we start with the A and goes in the normal order, when we finish the alphabet, we begin over by putting a 1 to the right, when it finishes we increase 1 by one and follow the alphabet. We always skip the "I" letter in both cases.

[15] These describe the orientation of the elliptical orbit. The argument of perihelion is the rotation angle of the ellipse around the Z-plane of x-y plane elliptical orbit. The inclination is the angle of the orbit with the x-y plane. The ascending nose is, according to us, the node where the orbiting object passes from the "southern" part of the orbit to the "northern" part of it in terms of the z-axis. Further information and schema can be found here.

[16] The initial position of the object in the ellipse.

[17] Check the DART mission from here, which hit Dimorphos.

GB, and power consumption increased from 30W to 50W, and the gain from 480 to 361. They had four different stations several hundred kilometers apart at first, then, they added 14 stations more in December 2023.

Katsuda et al.[34] reported the impacts of the explosive eruption of the Hunga Tonga-Hunga Ha'apai volcano on January 15, 2022, on the mesosphere and lower thermosphere with changes in x-ray observations from the Insight-HXMT X-ray astronomy satellite. The reported effects included a severe impact up to 1000 km away from the *epicenter* and weaker effects up to 7000 kilometers away.

Magnetohydrodynamics

Dymott et al.[35] studied the local magnetohydrodynamical (MHD) instabilities of differential rotations. They aimed to understand the poorly-characterized angular momentum transport in stellar zones by investigating the Goldreich-Schuburt-Fricke (GSF) and the MagnetoRotational Instability (MRI) with analytical and numerical methods. Later, they applied their models to the solar tachochline[18] and core of the red giants and reported the estimated significance of GSF or MRI on them under different local effective gravity vector-related angles for them.

Verma et al.[36] utilized a regularization technique for a complex limb darkening estimation and reported its accurate and precise results. They re-analyzed 43 lightcurves from the Kepler and Transiting Exoplanet Survey Satellite (TESS) missions. They used the BATMAN package, the Monte Carlo Markov Chain approach, and a new regularization routine to keep in check the parameters so that overfitting or underfitting would be minimal. Their model, BETMpy, was compared to the 1D non-magnetic models from the MPS-ATLAS and PHOENIX-COND and cautioned that potentially assuming a homogeneous magnetic field can introduce a discrepancy in the estimations, but overall, they still performed better with a 3D model than non-magnetic 1D models. These modifications reduced the standard deviations in astrometric fitting both in declination and right ascension angles. The orbital trajectory estimations were also improved, and the network was targeted to be expanded for more detailed analyses.

Huguet et al.[37] studied the planetary core solid-liquid phase changes with laboratory analyses. How the Earth's magnetic field is created and sustained was generally explained by the thermal convection, crystallization, and latent heat release. This review study stated the scalable properties of the solid-liquid phase change between the Earth's core and metallurgy and elaborated on mushy and slurry layers.

Presa et al.[38] studied the atmospheric escape with numerical 3D radiation-magnetohydrodynamic models. They generated 40 models from varying dipolar field strength of the planet and magnetic obliquity[19] and worked on them under the presence and absence of stellar winds, resulting in 80 models. They reported the transition from the magnetically unconfined regime of the night side tail to the polar escape with a changing planetary magnetic field. They also showed a way to link Lyman-α transitions and stellar wind characteristics, among many other interesting results.

[18] The transition region between the radiative interior and convective zone of stars with larger masses than 0.3 solar masses.

[19] The angle between the rotational and magnetic axes.

Last week in Chemistry

Author: Yasin Güray Hatipoğlu

The preprints summarized here were published between October 8 - October 14, 2024. They are more in nature of spectroscopy alone, and hence several studies regarding biochemistry, chromatography, and several other disciplines might be missed here.

Mass Spectroscopy

Paul[39] developed a novel analytical toolkit concept for the characterization and development of halogen-free flame retardants (the case study is phosphorus and phosphorus-nitrogen basis). They used thermogravimetric analysis[20] measurements to derive the surface ignition temperature and kinetic degradation parameters. Total volatile organic compounds were measured by Thermal Desorption/Gas Chromatography/Mass Spectrometry. They also analyzed the gas phase and condensed phase flame retardant content with the Inductively Coupled Plasma and surface Focused Mass Spectrometer. All these methods were necessary to construct the big picture from the generated gases (which shows the efficiency of the flame retardants), to see the thermal behavior of the material, and to check the phase distribution of the phosphorus.

Brungs et al.[40] reported a workflow to generate a multi-stage fragmentation (more than two consecutive mass spectrometry to further identify the fragmentations of the fragmentations from the analyte). They provide their workflows, codes, and generated libraries through GitHub repository links and Zenodo links. Their flow-injection multi-stage MS was done by the Vanquish duo UltraHPLC coupled to an Orbitrap ID-X. Data-dependent acquisition picked the three most intense ions for the aforementioned multi-stage MS.,

Danischewski et al.[41] attempted to mitigate the loss and contamination problems of commonly used electrostatic ion gates in mass spectrometry instruments with a novel atmospheric-pressure ion gate. They used ultrasonic piezoelectric speakers TCT40-16R/T. Its response time and gating efficiency were found adequate and cost-efficient.

Infrared Spectroscopy - IR

In a cocrystal polymorph synthesis with a custom ball-milling platform, Parlier et al.[42] combined Raman spectroscopy (WP 785 Raman Spectrometer from the Wasatch Photonics), thermal imaging (infrared, with a OPTRIS PI450i thermal imaging camera), and acoustic and high-speed optical video recording for the *operando* analysis. All mentioned methods complemented one another in figuring out the reaction mechanism. They also made *ex situ* characterizations with the FTIR, powderXRD, Raman, solid state NMR of ^{1}H and ^{13}C,

Electrochemistry

Nikzad et al.[43] developed a pipette-type thin layer electrode with a highly enhanced ampere/voltage ratio owing to the thin thickness of the confined solution for the electrochemistry operations. Not only did the pipette permit the subsequent analyses with the confined sample solution, but also it could monitor the reaction real-time via a hosted microelectrode. They benchmarked this utility with the oxidation of acetaminophen, acebutolol, and 2-acetyl-4-butyramidophenol. They reported the success of this method and pointed at the superior performance via an adjustable timeframe from minutes to hours.

Nuclear Magnetic Resonance - NMR

Boerkamp et al.[44] used NMR techniques to annotate oxidised lipid substructures. Firstly, using standard Bruker pulse programs, they recorded 950 MHz heteronuclear single quantum correlation, total correlation spectroscopy, and HSQC-TOCSY[21] and processed the spectra in TopSpin or MestReNova softwares. More spectra were collected at 600 MHz with the Bruker Avance III NMR spectrometer for 2D $^{1}H - ^{13}C$ heteronuclear multiple bond correlation in addition to the HSQC obtained at 950 MHz. Further focus was on hydroperoxyl hydrogen annotation and ROESY and HMBC spectra were taken for them. They reported that it is appropriate to deploy this NMR workflow for several related targets in oxylipidomic studies.

[20] TGA measures the *gravimetric* change with each thermal differential on the specimen. Desorbed/generated matter/gas can also be collected and analyzed.

[21] Further information on such 2-dimensional NMR techniques can be found here

Last week in Remote Sensing

Author: Yasin Güray Hatipoğlu

The preprints summarized here were published between October 8 - October 14, 2024. These are generally based on the preprints retrieved when "remote sensing" words are given between quotation marks within arXiv's cs.CV and similar cross-fields.

Segmentation

Haidar and Oramas trained an encoder, then, used this encoder to guide a single-label classification task and multi-label classification task for the hyperspectral image classification cases, respectively. The first stage of the contrastive-based encoder training was training with the unlabeled data and it created a pair, one original, the other a vertical or horizontal-transformed. Later, this resulted in two hidden representations (after ReLU activation and dropout layers) of the same location and these representations were to be maximally similar. Their contrastive loss function was the Normalised Temperature-scaled Cross Entropy Loss (NT-Xent). They, then, encoder results were fed to a previously-studied network for hyperspectral image analysis, and for the multi-label classification they used the Binary Cross Entropy with Logits Loss. They worked with the following four public data: Pavia University, Salinas, Housten 2013, and Houston 2018. The modification of their method, CL-tune, meaning the encoder's weights are also to be updated in the classification task, outperformed other models, and also "Joint" scheme when the autoencodeer and classifier were unified, was among the best performing networks.

Polewski et al.[45] came up with a solution to the problem of the natural resource monitoring requirements and the available benchmark dataset. They have a Bayesian approach that can be initialized with locations, masks, or bounding boxes, and the contour was initialized by projecting it onto the learned shape. They compared a vanilla eigenshape model and their deep shape model with the Mask R-CNN and K-net baselines on a precision forestry task and acquired the images themselves. Briefly, the task was finding the dead trees from the canopy images, and individual contours were to be covering the dead tree canopy. They evaluated the results via pixel-level and object-level metrics, and found that the deep shape model performed better. Another contour extraction study was done by Miao et al.[46]. They presented Direct Segment Anything Model - Remote Sensing version (DirectSAM-RS)[22] and they evaluated it under zero-shot and fine-tuning settings. They generated a large-scale dataset with Mask2Contour transformation from LoveDA, iSAID, DeepGlobe, and RefSegRS datasets, resulting in 34 thousand image-text-contour triplets. They found their novel approach successful and on par with the state-of-the-art.

Dong et al.[47] not only presented theCroBIM[23] framework to refer to segmentation in remote sensing tasks, but also provided RISBench large-scale benchmark dataset (52472 image-language-label triplets), and their model performed either the first- or the second-best. in many other datasets against the state-of-the-art several methods on the RRSIS-D, RefSegRS, and RISBench datasets.

Cao et al.[48] introduced a less computationally expensive state space model, the hybrid CVMH-UNet based on vision Mamba. In the end, their method was not the most computationally efficient one, albeit still comparatively closer to the efficient ones, but its accuracy was mostly the best for different cases (ISPRS Vaihingen and ISPRS Potsdam).

Modelling-Forecast

Garibov and Strielkowski[49] utilized AI and remote sensing techniques to retrieve suitable locations for tree planting. The identification step was done by the YOLOv8 and Retrieval-Augmented Generation-Gemini API combined approach. Then, they also incorporated time-series modeling and forecast to estimate the impact of reforestation on CO_2 emissions with the Holt-Winters. They used Google Earth Pro to access satellite imagery[24], and collected and compiled the climate, soil, and tree species data from various mediums. They reported that AI methods can indeed assist in this task successfully.

Object Detection

Ciocarlan et al.[50] worked on an object detection task with the self-supervised learning approach, where unlabeled datasets are used for training. They started with the COCO dataset for the benchmarking, then, for the domain-specific tasks, they used the VEDAI dataset for

[22] Based on a DirectSAM, the SegFormer encoder considered in previous issues of Science Ascend as well.

[23] They have a GitHub repository without the code yet.

[24] It is suspicious that they might have actually used aerial imagery, considering the spatial resolution of the provided several images.

small vehicle detection, and SSL-IR images collected from publicly available infrared datasets. They reported that different architectures' performances improved differently with different approaches (especially among instance discrimination and masked image modelling methods.

Shamsi et al.[51] considered the ship detection objects in marine environments via optical and hyperspectral data/methods, and reviewed and discussed the literature. In the end, they made a comparison table to aid in selecting the appropriate method for the task at hand.

Seth et al.[52] presented the Alberta Wells Dataset to aid in pinpointing oil and gas wells by remote sensing techniques. Their dataset included over 213000 wells (active, suspended, or abandoned). This dataset looks vastly superior to other available datasets with its sheer number. It is from Alberta, Canada, and the imagery source is Planet Labs. They also applied several algorithms for binary segmentation and binary object detection marks.

Zhang et al.[53] zeroed in on neglecting the global statistical information in the remote sensing images during the content-based remote sensing object retrieval tasks. They presented the generalized likelihood ratio test-based metric learning (GLRT-ML), which focused the network on the difficult sample in the training phase. For the real-world distribution shift between the training and test data, they introduced the clustering pseudo-labels-based fast parameter adaptation (CPLFPA) method. They followed these approaches in FGSRSI-23 and MAR20 datasets for ship and military aircraft recognitions, respectively, and reported that their novel methodology was highly effective.

Change Detection

Yu et al.[54] provided an extensive survey on the use and development of foundation models for image change detection tasks utilizing remote sensing data.

Xiao et al.[55] presented their bi-temporal Gaussian distribution feature-dependent network (BGFD) for more robust change detection in remote sensing. Firstly, to prevent overfitting and redundant feature capture, or domain knowledge change capture as the actual change, they used a new Gaussian Noise Domain Disturbance which perturbs the network. Their network had a feature dependency facilitation module with the mutual information difference loss and global attention mechanism integrated in it. The detail feature compensation balanced the global/detail loss-gains. They used four change detection-related datasets: DSIFN-CD, LEVIR-CD, SYSU-CD, and S2Looking. They compared the results to the FC-Siam-Conc, DTCDSCN, STANet, L-Unet, BIT, ChangeFormer, P2V, ChangeCLIP, and also the ground truth. Their approach was either the best or the second best performing.

Wang et al.[56] worked on change detection and change captioning in remote sensing, developed an algorithm that can track the change, caption them, and use both text and image to efficiently learn and process the data[25]. Their network is composed of three main steps: a transformer-based Siamese Encoder, which uses both pre-change and post-change images, this is followed by a ChangeLSTM module, and then, by the multi-task predictor that outputs a change captioning classifier and change detection classifier. They evaluated the performance of their model on the LEVIR-MCI dataset, and checked the method efficiency with five common change detection datasets and the DUBAI-change captioning dataset. Their method with the multi-task training was the best in all evaluations.

[25]The authors stated that the code related to the study will be published in this GitHub repo.

Last week in Environmental Chemistry

Author: Yasin Güray Hatipoğlu

The preprints summarized here were published between October 8 - October 14, 2024 in chemRxiv's Earth, Space, and Environmental chemistry preprints are being surveyed, and unfortunately, not many preprints are published under environmental topics in this field.

Pati et al.[57] studied the photochemical oxygen isotope fractionation. They used singlet oxygen ($^1O_2$) selective chromophoric dissolved organic matter (CDOM) to probe the relevant kinetics. The chemical quenchers were three aminoacids (L-histidine, L-methionine, L-tyrosine), and furfuryl alcohol. Rose bengal was used to generate $^1O_2$ after irradiation with a 30 W fluorescent light bulb at varying distances. They stated that photochemical-sourced isotope fractionation in oxygen is comparable to that of the typical DOM concentrations of aquatic environments.

Dettmann et al.[58] developed an automated parametrization way for the Vienna Soil Organic Matter Modeler 2 (VSOMM2). This VSOMM2 model, and similar approaches attempt to mitigate the complexity of the SOM structure estimation through modelling and simulation. Their parameterization started with the Swarm-CG for the individual fragments of smaller humic substances. For the coarse-grained models, the ETKDG (experimental-torsion basic knowledge distance geometry) approach was chosen. They cross-benchmarked the novel approach, and also used the GROMACS tool gmx velacc to calculate the vibrational power spectra of the fragments. This approach is also computationally more efficient than the previous tools.

Guo et al.[59] studied the photochemical generation pathways of trifluoroacetic acid (TFA). They focused on a degradation product of the fluoxetine, 4-TFMP and observed that ultraviolet-B light results in TFA generation in different pH environments. After radioactive-marked isotope tracking, they found that spontaneously-generated reactive oxygen species result in the formation of TFA via more than one mechanisms. Throughout the research study, they utilized HPLC-UV to measure 4-TFMP, fluoxetine, and other relevant compounds, the Ion Chromatography to detect fluoride and TFA, UHPLC-MS/MS to quantify the marked TFA, and UHPLC-Orbitrap-HRMS to quantify marked 4-TFMP and marked 4-TFMP, and ^{19}F NMR to

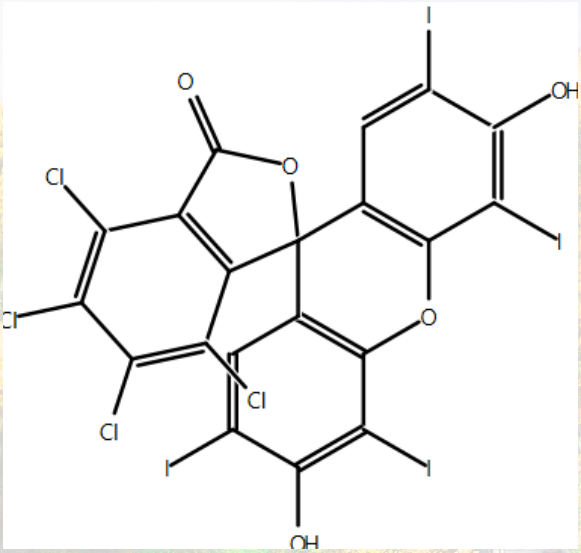

Figure 2: Molecular structure of rose bengal

elucidate the structure of the ^{19}F-bearing compounds. They also modelled the kinetics in the pseudo-first order way in the COPASI software, focusing on TFA.

The oxygen isotope ratio was measured by Gas Chromatography/Isotope Ratio Mass Spectrometry (GC/IRMS).

Last week in Data Decomposition/Transformation

Author: Yasin Güray Hatipoğlu

The preprints summarized here were published between October 8 - October 14, 2024. This is generally from arXiv's stat.ML or stat.ME cross-list. The section focuses on preprints heavily worked with or developed data decomposition/transformation techniques, such as principal component analysis (PCA) or Fourier Transformation.

Dimensional Reduction

Agterberg and Zhang[60] studied low Tucker rank tensors[26] having additive noise in the high-dimensions and examined the inference and uncertainty quantification, especially for the *higher-order orthogonal iteration* algorithm. They rigorously explained and tested their approaches and also provided relevant numerical simulations.

Kim and Oh[61] presented the gFreqPCA, the PCA for the graph frequency domain[27]. This is very relevant for the spatial analysis as well, but more on to the connections with the points-nodes than just locations, like a metro network. They reported that it was promising and had further room for development.

Time Series

Chang et al.[62] studied the canonical polyadic (CP)-decomposition for the high-dimensional time-series data. The CP-factor model is as follows:

$$Y_t = \mathrm{A}X_tB^T + \epsilon_t, \mathrm{t} \geq 1$$

X_t is the diagonal of the time series x_t, and A-B are factor loading matrices, Their algorithm was more robust and faster than the available ones in the literature.

Schär et al.[63] modelled dynamical systems driven by time-varying exogenous excitations, with the approach named the Functional Nonlinear AutoRegressive with eXogenous inputs (F-NARX). They chose the perspective from the continuous perspective to better understand and model the system response rather than discrete. They considered that this way was physically more meaningful and applied it to the eight-story building under wind loading, and three-story steel frame under seismic loading cases. They found their method successful under highly oversampled and more complex conditions of these cases.

Vrotsos and West[64] worked on the simultaneous graphical dynamic linear models (SGDLMs) theoretical background, structure, and application case on global macroecomomic time series datasets. Its representation resembles that of eigenvalue decomposition. Its core representation is:

$$(I - \Gamma_t)y_t = \mu_t + \nu_t \text{ with } \nu_t in N(0, \Lambda_t^{-1})$$

μ_t is trend, seasonality like terms, and Λ_t is positive residual diagonal-containing sparse matrix. They successfully used this model to interpret the focused dataset from the global macroeconomy.

Rocha and Garcia[65] improved the Variable Length Markov Chains with Exogenous Covariates (VLMCX) to make it incorporate time-independent and -invariant exogenous covariates, too. The dataset they worked on was the previous and subsequent Dengue rates, socioeconomic factors, and weather conditions.

Data Compression

Radünz et al.[66] constructed a data-independent Karhunen-Loève Transform (KLT) approximation to reduce the computational cost of the KLT, and selected the convenient 8 for the block length as it is common in the image and video compression. They applied the related KLT approximation methods available from the literature on the Lena image and a grass image. They were successful in developing faster and better-compressed results.

Modelling

Kwon et al.[67] introduced group Shapley values in the context of counterfactual simulations after setting its stage. They described the Shapley values, and then, introduced their novel group Shapley values to solve a constrained weighted least squares problem, with and without missing inputs. Then, they provided a machine learning use-case followed by the counterfactual simulation quantitative evaluation. They even go so far as to elaborate on two additional studies from the literature with their methods as well.

Nghiem and Hui[68] improved the sufficient dimension reduction technique for the clustered samples and made it more robust in that it did not assume the linear transformation was identical across all clusters. They incorporated the random effect heterogeneity among the clusters

[26] One can check the following UCLA slides on low-rank tensors and Tucker rank via here.

[27] They provided the data and R code here.

through a Grassmann manifold. They applied this method to the dataset of women life expectancy and socioeconomic variables.

Ge et al.[69] utilized principal component analysis in measurement error correction tasks for the spatial environmental exposure estimation analyses. One case study example was a person being near green areas, where this can be measured via Normalized Difference Vegetation Index (NDVI) from remote sensing data, and the depression onset. For the validation, GPS-tracked data were also available, while the actual dataset was statement and other less-certain sources. They also considered determining the measurement error model and stated that the entire workflow of the study is robust and beneficial for these tasks.

Selected Works From Machine Learning

Author: Oğuz Demirtaş

Ba et al. [70] released a new study for model calibration with synthetic data. They propose a new calibration method that achieves decreasing both accuracy and misclassification errors at the same time. The study, which is derived from the Probably Approximately Correct(PAC) learning framework, first derives the Expected Calibration Error(EC), which is a well-known metric to measure a model's prediction to the accuracy, to see the possibility of achieving high accuracy and low ECE. Then LLM-generated synthetic data is put into the dataset. The size of the syntethic data in the training set is between 7%-18%. They report that after four different natural language processing tasks, 34% increase in accuracy and 33% decrease in ECE. They also emphasize in the article that using synthetic data is necessary for model calibration.

Calatvara-Nicolas and Mozos [71] proposed a new adversarial deep learning framework for the human activity recognition(HAR) problem. They studied HAR to recognize the activities of daily living (ADL), which is one of the fields in which HAR is applied. The framework they propose includes both the user dimension and activity dimension. It means they build a binary classification task that detects the activity features coming from the same person and the same activity or from a different person but still the same activity. This information flow creates a deep feature space for activities even if they come from different people and makes classifying the activities easier. The study reports that their discrimination task has better classification results compared to other well-known tasks for ADL.

Rigter et al. [72], from Microsoft Research, UK, developed an approach called AVID to generate videos using a pretrained video model without learning the parameters of the model. In this work, they assume that they have access to the noise predictions of the pretrained diffusion model. AVID, as a domain-specific adapter, modifies these noise predictions and generates video. They tested AVID on video game data generated by Procgen and RT1 and reported that AVID can generate accurate videos without accessing parameters of the pretrained diffusion model.

References

[1] Nora Hänni, Kathrin Altwegg, Michael Combi, Stephen A. Fuselier, Johan De Keyser, Niels F. W. Ligterink, Martin Rubin, and Susanne F. Wampfler. Evidence for abiotic dimethyl sulfide in cometary matter. *arXiv*, 2024.

[2] A. Sharma, E. Stonkutė, A. Drazdauskas, R. Minkevičiūtė, Š. Mikolaitis, G. Tautvaišienė, and T. Narbuntas. Chemical composition of planetary hosts: C, n, and α-element abundances. *arXiv*, 2024.

[3] Jessica L. Diamond and Richard J. Parker. Formation of jupiter-mass binary objects through photoerosion of fragmenting cores. *arXiv*, 2024.

[4] K. L. Luhman, C Alves de Oliveira, I. Baraffe, G. Chabrier, E. Manjavacas, R. J. Parker, and P. Tremblin. Jwst/nirspec observations of brown dwarfs in the orion nebula cluster. *arXiv*, 2024.

[5] Gregory J. Cooke and Nikku Madhusudhan. Considerations for photochemical modeling of possible hycean worlds. *arXiv*, 2024.

[6] Quanyi Liu, Wei Zhu, Kento Masuda, Jessica E. Libby-Roberts, Aaron Bello-Arufe, and Caleb I. Canas. An extremely low-density exoplanet spins slow. *arXiv*, 2024.

[7] Lena Noack, Caroline Dorn, and Philipp Baumeister. Chapter 10031. surfaces and interiors. *arXiv*, 2024.

[8] G. Conzo, N. Leiner, K. Lynch, M. Moriconi, N. Ruocco, and T. Scarmato. Tic 393818343 c: Discovery and characterization of a neptune-like planet in the delphinus constellation. *arXiv*, 2024.

[9] S. L. Casewell, M. R. Burleigh, R. Napiwotzki, M. Zorotovic, P. Bergeron, J. R. French, J. J. Hermes, F. Faedi, and K. L. Lawrie. The evolutionary history of gd1400, a white dwarf-brown dwarf binary. *arXiv*, 2024.

[10] Mario Damiano, Stuart Shaklan, Renyu Hu, Brian Dunne, Angelle Tanner, Aly Nida, Joseph C. Carson, Sergi R. Hildebrandt, and Doug Lisman. Starshade exoplanet data challenge: What we learned. *arXiv*, 2024.

[11] Abbigail K. Elms, Nicola Pietro Gentile Fusillo, Pier-Emmanuel Tremblay, Ralph C. Bohlin, Mark A. Hollands, Snehalata Sahu, Mairi W. O'Brien, Susana Deustua, and Tim Cunningham. A network of cooler white dwarfs as infrared standards for flux calibration. *arXiv*, 2024.

[12] Florian Lalande, Elizabeth Tasker, and Kenji Doya. Estimating exoplanet mass using machine learning on incomplete datasets. *arXiv*, 2024.

[13] H. J. Deeg. Impact of exoplanet science on society: Professional contributions, citizen science engagement and public perception. *arXiv*, 2024.

[14] Jason T. Wright, Macy Huston, Aidan Groenendaal, Lennon Nichol, and Nick Tusay. Seti in 2022. *arXiv*, 2024.

[15] Vinicius M. Placco, Arvind F. Gupta, Felipe Almeida-Fernandes, Sarah E. Logsdon, Jayadev Rajagopal, Erika M. Holmbeck, Ian U. Roederer, John Della Costa, Pipa Fernandez, Eli Golub, Jesus Higuera, Yatrik Patel, Susan Ridgway, and Heidi Schweiker. Bd+44 493: Chemo-dynamical analysis and constraints on companion planetary masses from wiyn/neid spectroscopy. *arXiv*, 2024.

[16] Sean K. Terry, Jean-Philippe Beaulieu, David P. Bennett, Aparna Bhattacharya, Jon Hulberg, Macy J. Huston, Naoki Koshimoto, Joshua W. Blackman, Ian A. Bond, Andrew A. Cole, Jessica R. Lu, Clément Ranc, Natalia E. Rektsini, and Aikaterini Vandorou. A candidate high-velocity exoplanet system in the galactic bulge. *arXiv*, 2024.

[17] James Kirk, Eva-Maria Ahrer, Alastair B. Claringbold, Maria Zamyatina, Chloe Fisher, Mason McCormack, Vatsal Panwar, Diana Powell, Jake Taylor, Daniel P. Thorngren, Duncan A. Christie, Emma Esparza-Borges, Shang-Min Tsai, Lili Alderson, Richard A. Booth, Charlotte Fairman, Mercedes López-Morales, N. J. Mayne, Annabella Meech, Paul Molliere, James E. Owen, Anna B. T. Penzlin, Denis E. Sergeev, Daniel Valentine, Hannah R. Wakeford, and Peter J. Wheatley. Bowie-align: Jwst reveals hints of planetesimal accretion and complex sulphur chemistry in the atmosphere of the misaligned hot jupiter wasp-15b. *arXiv*, 2024.

[18] Daniel Valentine, Hannah R. Wakeford, Ryan C. Challener, Natasha E. Batalha, Nikole K. Lewis, David Grant, Elijah Mullens, Lili Alderson, Jayesh Goyal, Ryan J. MacDonald, Erin M. May, Sara Seager, Kevin B. Stevenson, Jeff A. Valenti, Natalie H. Allen, Néstor Espinoza, Ana Glidden, Amélie Gressier, Jingcheng Huang, Zifan Lin, Douglas Long, Dana R. Louie,

Mark Clampin, Marshall Perrin, Roeland P. van der Marel, and C. Matt Mountain. Jwst-tst dreams: Non-uniform dayside emission for wasp-17b from miri/lrs. *arXiv*, 2024.

[19] Amélie Gressier, Ryan J. MacDonald, Néstor Espinoza, Hannah R. Wakeford, Nikole K. Lewis, Jayesh Goyal, Dana R. Louie, Michael Radica, Natasha E. Batalha, Douglas Long, Erin M. May, Elijah Mullens, Sara Seager, Kevin B. Stevenson, Jeff A. Valenti, Lili Alderson, Natalie H. Allen, Caleb I. Cañas, Ryan C. Challener, Knicole Colòn, Ana Glidden, David Grant, Jingcheng Huang, Zifan Lin, Daniel Valentine, C. Matt Mountain, Laurent Pueyo, Marshall D. Perrin, and Roeland P. van der Marel. Jwst-tst dreams: A super-solar metallicity in wasp-17 b dayside atmosphere from niriss soss eclipse spectroscopy. *arXiv*, 2024.

[20] Vatsal Panwar, Matteo Brogi, Siddharth Gandhi, Heather Cegla, and Marina Lafarga. The mystery of water in the atmosphere of τ boötis b continues: insights from revisiting archival crires observations. *arXiv*, 2024.

[21] Panayotis Lavvas, Sophia Paraskevaidou, and Anthony Arfaux. Atmospheric characterisation of gj1214b from transit and eclipse observations. *arXiv*, 2024.

[22] Reza Ashtari, Kevin B. Stevenson, David Sing, Mercedes Lopez-Morales, Munazza K. Alam, Nikolay K. Nikolov, and Thomas M. Evans-Soma. The clear sky corridor: Insights towards aerosol formation in exoplanets using an ai-based survey of exoplanet atmospheres. *arXiv*, 2024.

[23] Hajime Kawahara, Yui Kawashima, Shotaro Tada, Hiroyuki Tako Ishikawa, Ko Hosokawa, Yui Kasagi, Takayuki Kotani, Kento Masuda, Stevanus Nuguroho, Motohide Tamura, Hibiki Yama, Daniel Kitzmann, Nicolas Minesi, and Brett M. Morris. Differentiable modeling of planet and substellar atmosphere: High-resolution emission, transmission, and reflection spectroscopy with exojax2. *arXiv*, 2024.

[24] Tamami Okamoto and Shigeru Ida. Effect of different stickiness between icy and silicate particles on carbon depletion in protoplanetary disks. *arXiv*, 2024.

[25] Urs Schäfer, Anders Johansen, Troels Haugbølle, and Åke Nordlund. Thousands of planetesimals: Simulating the streaming instability in very large computational domains. *arXiv*, 2024.

[26] Yao Tang, Jonathan J. Fortney, and Ruth Murray-Clay. Assessing core-powered mass loss in the context of early boil-off: Minimal long-lived mass loss for the sub-neptune population. *arXiv*, 2024.

[27] Sivan Ginzburg, Re'em Sari, and Abraham Loeb. Blackbody radiation from isolated neptunes. *The Astrophysical Journal Letters*, 822(1):L11, April 2016.

[28] P. Nazari, A. D. Sellek, and G. P. Rosotti. Hidden under a warm blanket: If planets existed in protostellar disks, they would hardly produce observable substructures. *arXiv*, 2024.

[29] Himanshu Tyagi, Manoj P., Mayank Narang, S T. Megeath, Will Robson M. Rocha, Nashanty Brunken, Adam E. Rubinstein, Robert A. Gutermuth, Neal J. Evans, Ewine van Dishoeck, Sam Federman, Dan M. Watson, David A. Neufeld, Guillem Anglada, Henrik Beuther, Alessio Caratti o Garatti, Leslie W. Looney, Pooneh Nazari, Mayra Osorio, Thomas Stanke, Yao-Lun Yang, Tyler L. Bourke, William J. Fischer, Elise Furlan, Joel D. Green, Nolan Habel, Pamela Klaassen, Nicole Karnath, Hendrik Linz, James Muzzerolle, John J. Tobin, Prabhani Atnagulov, Rohan Rahatgaonkar, Patrick D. Sheehan, Katerina Slavicinska, Amelia M. Stutz, Łukasz Tychoniec, and Scott J. Wolk. Jwst-ipa: Chemical inventory and spatial mapping of ices in the protostar hops370 – evidence for an opacity hole and thermal processing of ices. *arXiv*, 2024.

[30] Pekka Janhunen. Launching mass from the moon helped by lunar gravity anomalies. *arXiv*, 2024.

[31] Aster G. Taylor, Darryl Z. Seligman, Matthew J. Holman, Peter Veres, Davide Farnocchia, Nikole Lewis, Marco Micheli, and Jason T. Wright. Strong nongravitational accelerations and the potential for misidentification of near-earth objects. *arXiv*, 2024.

[32] Ethan R. Burnett, Iosto Fodde, and Fabio Ferrari. Exploring tidal dissipation in rubble pile binary secondaries using a discrete element model. *arXiv*, 2024.

[33] Z. Li, H. Zou, J. Liu, J. Ma, Q. Meng, Y. Cai, X. Zhao, X. Li, Z. Tu, B. Zhang, R. Wang, S. Wang, and F. Lu. A multi-station meteor monitoring (m^3) system. ii. system upgrade and a pathfinder network. *arXiv*, 2024.

[34] Satoru Katsuda, Hiroyuki Shinagawa, Hitoshi Fujiwara, Hidekatsu Jin, Yasunobu Miyoshi, Yoshizumi Miyoshi, Yuko Motizuki, Motoki Nakajima, Kazuhiro Nakazawa, Kumiko K. Nobukawa, Yuichi Otsuka, Atsushi Shinbori, Takuya Sori, Chihiro Tao, Makoto S. Tashiro, Yuuki Wada, and Takaya Yamawaki. X-raying neutral density disturbances in the mesosphere and lower thermosphere induced by the 2022 hunga-tonga volcano eruption-explosion. *arXiv*, 2024.

[35] Robert W. Dymott, Adrian J. Barker, Chris A. Jones, and Steven M. Tobias. Local stability of differential rotation in magnetised radiation zones and the solar tachocline. *arXiv*, 2024.

[36] Kuldeep Verma, Pierre F. L. Maxted, Anjali Singh, H. G. Ludwig, and Yashwardhan Sable. A regularisation technique to precisely infer limb darkening using transit measurements: can we estimate stellar surface magnetic fields? *arXiv*, 2024.

[37] Ludovic Huguet, Quentin Kriaa, Thierry Alboussière, and Michael Le Bars. Solid-liquid phase change in planetary cores. *arXiv*, 2024.

[38] Andrés Presa, Florian A. Driessen, and Aline A. Vidotto. Atmospheric escape in hot jupiters under sub-alfvénic interactions. *arXiv*, 2024.

[39] Swaraj Paul. Novel analytical toolkit concept for the characterization and development of halogen free flame retardants (hffr): A case study with p and pn based flame retardants. 2024.

[40] Corinna Brungs, Robin Schmid, Steffen Heuckeroth, Aninda Mazumdar, Matúš Drexler, Pavel Šácha, Pieter C Dorrestein, Daniel Petras, Louis-Felix Nothias, Václav Veverka, et al. Efficient generation of open multi-stage fragmentation mass spectral libraries. 2024.

[41] Julia Danischewski, Yi You, Lauren Bauer, Jens Riedel, and Jacob Shelley. Use of resonant acoustic fields as atmospheric-pressure ion gates. 2024.

[42] Eloïse Marie Samantha Parlier, Kinann Al Amir, Thomas-Xavier Métro, Pierre Granjon, Danielle Laurencin, and César Leroy. Listening to the formation of cocrystals and transformation of polymorphs in mechanochemistry through advanced operando acoustic analysis and real-time methods. 2024.

[43] Nastaran Nikzad, Buwanila T Punchihewa, Vidit Minda, William G Gutheil, and Mohammad Rafiee. An electrochemical pipette for the study of drug metabolite. 2024.

[44] Vincent JP Boerkamp, Marie Hennebelle, Jean-Paul Vincken, and John van Duynhoven. Comprehensive molecular mapping of vegetable oil autoxidation products by nmr-based oxylipidomics. 2024.

[45] Przemyslaw Polewski, Jacquelyn Shelton, Wei Yao, and Marco Heurich. Segmenting objects with bayesian fusion of active contour models and convnet priors. *arXiv*, 2024.

[46] Shiyu Miao, Delong Chen, Fan Liu, Chuanyi Zhang, Yanhui Gu, Shengjie Guo, and Jun Zhou. Prompting directsam for semantic contour extraction in remote sensing images. *arXiv*, 2024.

[47] Zhe Dong, Yuzhe Sun, Yanfeng Gu, and Tianzhu Liu. Cross-modal bidirectional interaction model for referring remote sensing image segmentation. *arXiv*, 2024.

[48] Yice Cao, Chenchen Liu, Zhenhua Wu, Wenxin Yao, Liu Xiong, Jie Chen, and Zhixiang Huang. Remote sensing image segmentation using vision mamba and multi-scale multi-frequency feature fusion. *arXiv*, 2024.

[49] Seymur Garibov and Wadim Strielkowski. Underutilized land and sustainable development: effects on employment, economic output, and mitigation of co2 emissions. *arXiv*, 2024.

[50] Alina Ciocarlan, Sidonie Lefebvre, Sylvie Le Hégarat-Mascle, and Arnaud Woiselle. Self-supervised learning for real-world object detection: a survey. *arXiv*, 2024.

[51] Alyazia Al Shamsi, Alavikunhu Panthakkan, Saeed Al Mansoori, and Hussain Al Ahmad. Advancements in ship detection: Comparative analysis of optical and hyperspectral sensors. *arXiv*, 2024.

[52] Pratinav Seth, Michelle Lin, Brefo Dwamena Yaw, Jade Boutot, Mary Kang, and David Rolnick. Alberta wells dataset: Pinpointing oil and gas wells from satellite imagery. *arXiv*, 2024.

[53] Linping Zhang, Yu Liu, Xueqian Wang, Gang Li, and You He. Glrt-based metric learning for remote sensing object retrieval. *arXiv*, 2024.

[54] Zihan Yu, Tianxiao Li, Yuxin Zhu, and Rongze Pan. Exploring foundation models in remote sensing image change detection: A comprehensive survey. *arXiv*, 2024.

[55] Yi Xiao, Bin Luo, Jun Liu, Xin Su, and Wei Wang. Bi-temporal gaussian feature dependency guided change detection in remote sensing images. *arXiv*, 2024.

[56] Yuduo Wang, Weikang Yu, Michael Kopp, and Pedram Ghamisi. Changeminds: Multitask framework for detecting and describing changes in remote sensing. *arXiv*, 2024.

[57] Sarah G Pati, Lara M Brunner, Martin Ley, and Thomas B Hofstetter. Oxygen isotope fractionation of o2 consumption through abiotoic photochemical singlet oxygen formation pathways. 2024.

[58] Lorenz Dettmann, Oliver Kühn, and Ashour A Ahmed. An automated parametrization approach for coarse-graining soil organic matter molecules. 2024.

[59] Zhefei Guo, Azka Attar, Qiqige Qiqige, Rylan Lundgren, and Shira Joudan. Photochemical formation of trifluoroacetic acid: Mechanistic insights into a fluoxetine-related aryl-cf3 compound. 2024.

[60] Joshua Agterberg and Anru Zhang. Statistical inference for low-rank tensors: Heteroskedasticity, subgaussianity, and applications. *arXiv*, 2024.

[61] Kyusoon Kim and Hee-Seok Oh. Principal component analysis in the graph frequency domain. *arXiv*, 2024.

[62] Jinyuan Chang, Yue Du, Guanglin Huang, and Qiwei Yao. Identification and estimation for matrix time series cp-factor models. *arXiv*, 2024.

[63] Styfen Schär, Stefano Marelli, and Bruno Sudret. Feature-centric nonlinear autoregressive models. *arXiv*, 2024.

[64] Mike West and Luke Vrotsos. Dynamic graphical models: Theory, structure and counterfactual forecasting. *arXiv*, 2024.

[65] Marília Gabriela Rocha and Nancy L. Garcia. Predicting dengue outbreaks: A dynamic approach with variable length markov chains and exogenous factors. *arXiv*, 2024.

[66] A. P. Radünz, D. F. G. Coelho, F. M. Bayer, R. J. Cintra, and A. Madanayake. Fast data-independent klt approximations based on integer functions. *arXiv*, 2024.

[67] Yongchan Kwon, Sokbae Lee, and Guillaume A. Pouliot. Group shapley value and counterfactual simulations in a structural model. *arXiv*, 2024.

[68] Linh H. Nghiem and F. K. C. Hui. Random effects model-based sufficient dimension reduction for independent clustered data. *arXiv*, 2024.

[69] Lin Ge, Ce Yang, David Zucker, Jiaxuan Li, Donna Spiegelman, and Molin Wang. Measurement error correction for spatially defined environmental exposures in survival analysis. *arXiv*, 2024.

[70] Yang Ba, Michelle V Mancenido, and Rong Pan. Fill in the gaps: Model calibration and generalization with synthetic data. *arXiv preprint arXiv:2410.10864*, 2024.

[71] Francisco M Calatrava-Nicolás and Oscar Martinez Mozos. Deep adversarial learning with activity-based user discrimination task for human activity recognition. *arXiv preprint arXiv:2410.12819*, 2024.

[72] Marc Rigter, Tarun Gupta, Agrin Hilmkil, and Chao Ma. Avid: Adapting video diffusion models to world models. *arXiv preprint arXiv:2410.12822*, 2024.